‑ ‑

Asymptotic evolution of nonlinear Landau damping

‑ ‑

Brunetti, Maura; Califano, F.; Pegoraro, F.

Asymptotic evolution of nonlinear Landau damping

M. Brunetti,[1,2] F. Califano,[2] and F. Pegoraro[1,2]

[1]*Dipartimento Fisica, Università di Pisa, Pisa, Italy*
[2]*Istituto Nazionale Fisica della Materia, Sezione A, Pisa, Italy*
(Received 6 December 1999; revised manuscript received 4 April 2000)

The long-time evolution of nonlinear Landau damping in collisionless plasmas is analyzed by solving the Vlasov-Poisson system numerically. The value of the parameter marking the transition between Landau's and O'Neil's regimes is determined and compared with analytical results. The long-time evolution of a finite-amplitude electric field with wavelength λ equal to the length of the simulation box L is given by a superposition of two counterpropagating ''averaged'' Bernstein-Greene-Kruskal (BGK) waves. When $L > \lambda$ and longer wavelength modes can be excited, the BGK waves correspond to an intermediate regime that is eventually modified by the excitation of the sideband instability. Ions dynamics is found not to affect these behaviors significantly.

PACS number(s): 52.35.Fp, 52.35.Mw, 52.35.Qz

I. INTRODUCTION

The self-consistent damping of longitudinal waves in collisionless plasmas is a classic fundamental problem in the study of nonlinear wave-particle interaction processes.

In the linear regime, when a spatially uniform plasma with equilibrium electron distribution function (EDF) $f^{eq}(v)$ is perturbed by a small-amplitude electrostatic disturbance, the Landau's analysis [1] predicts that the time-asymptotic evolution of the electric field exhibits exponential damping (or growth) as well as oscillatory behavior. The damping (or growing) rate γ_k is proportional to the derivative with respect to v of the equilibrium EDF calculated at the phase velocity v_{ph} of the electrostatic wave.

In the case of a Maxwellian equilibrium EDF $f^{eq}(v) = f^M(v)$, a long-wavelength electron plasma oscillation with $k\lambda_D \ll 1$, where λ_D is the Debye length and k is the wave number, decays with time on a scale that is large compared to that of the oscillation time. However, even in the case of ''small''-amplitude perturbations, the linear analysis breaks down for $t > t_p$, t_p being the particle trapping time scale that depends on the electric-field amplitude E as $t_p = 1/\sqrt{kE}$ in normalized units [see below Eq. (2.2)]. Thus, Landau's linear solution holds at large times only if initially the condition $t_d \ll t_p$ is satisfied, where t_d is the damping time scale. In the opposite limit $t_d \gg t_p$, O'Neil [2] has shown that the energy exchange between the wave and the particles with velocities $v \simeq v_{ph}$ trapped in the wave prevents the complete damping of the wave that reaches a constant nonzero value asymptotically.

Recently, the existence of a critical initial perturbation amplitude, which marks the transition between these two different asymptotic regimes, has been proved in the limit of small-amplitude waves [3] and the analytical expression of the asymptotic wave amplitude a_{fin} has been given in the case of a sinusoidal perturbation of a linearly stable equilibrium. In this limit, the general solution for the asymptotic electric field has been found to be a finite superposition [4] of traveling Bernstein-Greene-Kruskal (BGK) waves [5] plus higher-order terms [see Eq. (9) of Ref. [3]], a subject that has been recently studied in many numerical and theoretical works. In Ref. [6], a generic longitudinal plasma-wave perturbation was found to decay as $1/t$ and not to be stopped by the nonlinear effects of particle trapping and BGK wave formation. However, the numerical results presented in Ref. [7], for a single value of the perturbation amplitude, and the results of Ref. [8], which show that the damping rate vanishes for $t \to \infty$ for a wide class of nonlinear waves, contradict the conclusions of Ref. [6].

Here, we report the results of a systematic numerical study of the Vlasov-Poisson equations in the intermediate range where the restrictions assumed in the papers of Landau ($t_d \ll t_p$) and O'Neil ($t_d \gg t_p$) do not apply.

The ratio between the time scales characterizing the system $q = t_p/t_d$ is analyzed as a function of the initial perturbation amplitude ϵ, and the critical perturbation amplitude ϵ^* marking the transition between Landau's and O'Neil's scenarios is determined and discussed. For small-amplitude initial conditions, a comparison with the analytical results in Ref. [3] is performed.

When $\epsilon > \epsilon^*$, the asymptotic state of an initial perturbation with wavelength λ equal to the length of the simulation box L is found to be a superposition of two counterpropagating ''averaged'' BGK waves. Filaments of increasingly smaller size are also formed in phase space due to phase mixing, but they gradually disappear because of the finite resolution of the simulations. We show that the asymptotic state is a superposition of averaged BGK waves, also in the case of large-amplitude waves.

For $L > \lambda$, such that modes with longer wavelengths can be excited, the onset of the sideband instability changes the asymptotic evolution of the system and the BGK solutions play the role of an intermediate regime.

Finally, we discuss whether the behavior of such systems changes when the ion dynamics is included.

The paper is organized as follows. In Sec. II, the basic equations are given and the properties of the code employed are discussed. In Sec. III, the numerical results concerning the determination of the critical value ϵ^* are presented and discussed. The formation of averaged BGK waves, the onset

PRE <u>62</u>   4109

TABLE I. Normalized time scales and parameters of the simulations with $v_{th}=0.1$, $k=4$, $L=2\pi/k$, for $\epsilon>\epsilon^*$.

ϵ	a_{in}	t_p	t_d	q	a_{fin}
0.015	0.0019	11.5	15.1	0.76	2.2×10^{-5}
0.017	0.002125	10.8	15.1	0.72	6.0×10^{-5}
0.018	0.00225	10.5	15.1	0.70	7.0×10^{-5}
0.020	0.0025	10.0	15.1	0.66	9.3×10^{-5}
0.025	0.003125	8.9	15.1	0.59	1.7×10^{-4}
0.03	0.00375	8.2	15.1	0.54	2.8×10^{-4}
0.04	0.005	7.1	15.1	0.47	5.1×10^{-4}
0.05	0.0062	6.3	14.3	0.44	8.2×10^{-4}
0.07	0.0088	5.3	13.7	0.39	1.1×10^{-3}
0.08	0.01	5.0	13.3	0.38	1.5×10^{-3}
0.1	0.0125	4.5	12.5	0.36	2.2×10^{-3}
0.2	0.025	3.2	9.1	0.35	5.5×10^{-3}
0.25	0.03125	2.8	7.7	0.37	8.0×10^{-3}
0.3	0.0375	2.6	6.7	0.39	8.8×10^{-3}

of the sideband instability, and the role of ion dynamics are presented in Sec. IV. Conclusions are drawn in Sec. V.

II. BASIC EQUATIONS

We solve the one-dimensional Vlasov-Poisson system of equations numerically:

$$\frac{\partial f}{\partial t}+v\frac{\partial f}{\partial x}-E\frac{\partial f}{\partial v}=0, \tag{2.1}$$

$$\frac{\partial E}{\partial x}=1-\int_{-\infty}^{+\infty}f\,dv, \tag{2.2}$$

where $f(x,v,t)$ is the EDF and $E(x,t)$ is the electric field, which at $t=0$, is given by

$$E(x,0)=2\,a_{in}\sin(kx). \tag{2.3}$$

In Eqs. (2.1) and (2.2) and in the following, time is normalized to the inverse of the electron plasma frequency ω_{pe}, velocity to the speed of light c, and consequently, E to $mc\omega_{pe}/e$ and f to the equilibrium particle density n_0. At first, we assume that the ions form a fixed, neutralizing background. Oscillations are excited by initializing Fourier spatial modes with wave number k and $-k$:

$$f(x,v,0)=f^M(v)[1+\epsilon\cos(kx)], \tag{2.4}$$

where ϵ is the perturbation amplitude, related to the initial electric-field amplitude a_{in} as $\epsilon=2ka_{in}$, and $f^M(v)$ is the Maxwellian EDF,

$$f^M(v)=\frac{1}{\sqrt{2\pi}v_{th}}\exp[-v^2/(2v_{th}^2)]. \tag{2.5}$$

Here v_{th} is the thermal velocity.

The Vlasov-Poisson equations are integrated numerically in the 1-D 1-V phase space (x,v) by using the well-known "splitting scheme" developed in Ref. [9] in the electrostatic limit. The Poisson equation is integrated in the Fourier space

by using a standard fast Fourier transform algorithm coupled to the fourth-order Runge-Kutta scheme.

The number of points used in the simulations are typically $N_x=256$, $N_v=3000$ with $dt\simeq0.0025$. The numerical phase space is given by $0\leq x<L$, $-v_{max}\leq v\leq v_{max}$, where L is the maximum length of the space interval and v_{max} the maximum velocity that can be reached by the particles. Periodic boundary conditions are used in the space direction. The simulation is stopped if the particles are accelerated up to v_{max}.

The code has been tested in many well-known electrostatic problems, as, for example, plasma waves, Landau damping, two-stream instability, and Best's oscillations.

III. CRITICAL INITIAL PERTURBATION AMPLITUDE

We present a number of simulations (some of which are listed in Table I) with $v_{max}=0.6$, $\lambda=2\pi/k=L$, and with different values of the initial perturbation amplitude ϵ. We set the thermal velocity to $v_{th}=0.1$ in order to describe plasmas with a nonrelativistic temperature, and the initially perturbed wave number to $k=4$. The evolution of the system is investigated up to $t\simeq2500\omega_{pe}^{-1}$. The perturbation amplitude ϵ, the initial wave amplitude $a_{in}=\epsilon/(2k)$, the trapping time $t_p=1/\sqrt{ka_{in}}=\sqrt{2/\epsilon}$, the damping time t_d, their ratio $q=t_p/t_d$, and the large-time wave amplitude a_{fin} are given in Table I. Note that the definition of t_p given before is used conventionally also for large-amplitude waves and that t_d is estimated numerically from the simulations.

When the initial amplitude of the electric field is sufficiently small, we can calculate the damping rate using linear theory [1,10]. For $k=4$, we find for the Landau damping rate $\gamma_L=-0.0661$, and $t_L=1/|\gamma_L|=15.1$. However, as can be seen from Table I (in agreement with [11]), t_d is different from t_L in all the simulations with $\epsilon>0.04$, since the corresponding amplitude cannot be considered as "small."

For very small perturbations $t_d=t_L=$const, while $t_p=\sqrt{2/\epsilon}$, so that $q\to\infty$ as $\epsilon\to0$. In Fig. 1(a), we plot the asymptotic amplitude a_{fin} of the electric field versus the initial perturbation amplitude ϵ, at fixed wave number $k=4$.
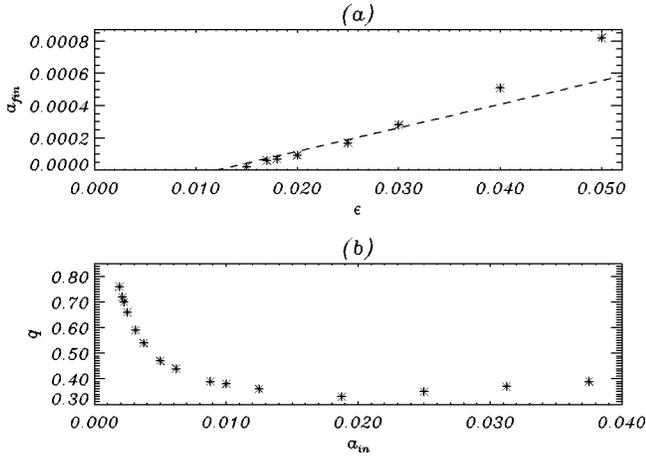
FIG. 1. (a) Final electric-field amplitude a_{fin} as a function of the initial perturbation amplitude ϵ; (b) $q = t_p/t_d$ plotted versus the initial electric-field amplitude a_{in}.

The dashed line corresponds to the analytical expression of the asymptotic amplitude given by Eq. (19) in Ref. [3], which in our units and for an initial perturbation of the form given in Eq. (2.4), reads (for $v_{th} = 0.1$ and $v_{ph} = 0.31$),

$$a_{fin} = \frac{4\pi \ v_{th}^2}{(v_{ph}^2/v_{th}^2 - 1)}(\epsilon - \epsilon^*) \simeq 0.0146(\epsilon - \epsilon^*), \quad (3.1)$$

where ϵ^* is the critical initial perturbation amplitude that marks the transition between Landau's and O'Neil's scenarios. The analytical expression of ϵ^* is reported in Ref. [3] in terms of the transient part of the electric field. The analytical values a_{fin} of Eq. (3.1) [dashed line in Fig. 1(a)] agree with our numerical results in the limit of small initial perturbation amplitudes $\epsilon < 0.04$ if we set $\epsilon^* \simeq 0.012$, which corre-

sponds to $q^* = \sqrt{2/\epsilon^*}/t_d \simeq 0.85$. For initial perturbations with $\epsilon < \epsilon^*$, the field amplitude is completely damped. Thus, this method allows us to find the critical value ϵ^*, avoiding the regime of very small initial perturbations, where the simulations are particularly delicate since the electric-field amplitude becomes so small that a very high numerical resolution is necessary. Nevertheless, setting $N_x = 256$ and $N_v = 3000$, we find that the plasma oscillations are completely destroyed and the field amplitude reaches the noise level when $\epsilon \leq 0.01$, according to the critical value of ϵ^* and q^* found by using the different method described before. The critical initial value q^* differs from those previously predicted in Ref. [12], which were obtained for lower resolution and shorter times.

In Table I, only the simulation results for $\epsilon > \epsilon^*$ are listed. We find that there is a minimum in q as a function of ϵ in the parameter range considered, as can be seen in Fig. 1(b).

IV. AVERAGED BGK WAVES, SIDEBAND INSTABILITY, AND ROLE OF ION DYNAMICS

When the initial perturbation amplitude is such that $\epsilon > \epsilon^*$, nonlinear effects come into play and the electric-field amplitude oscillates at large times around a constant nonzero value a_{fin}. For $\epsilon = 0.05$, the results are in agreement with Ref. [7]. After the initial linear damping of the wave, two vortices appear in phase space, centered in $v = \pm v_{ph}$, and propagate in opposite directions. In order to analyze how these results depend on the numerical resolution used in our simulations, we have performed runs with different numbers of grid points N_x.

In Fig. 2, we plot the spatial Fourier component E_k with $k = 4$ versus t for $\epsilon = 0.1$, large times, and different values of N_x (only $E_k > 0$ is shown for symmetry reasons). We note that the time at which the damping stops and the electric-
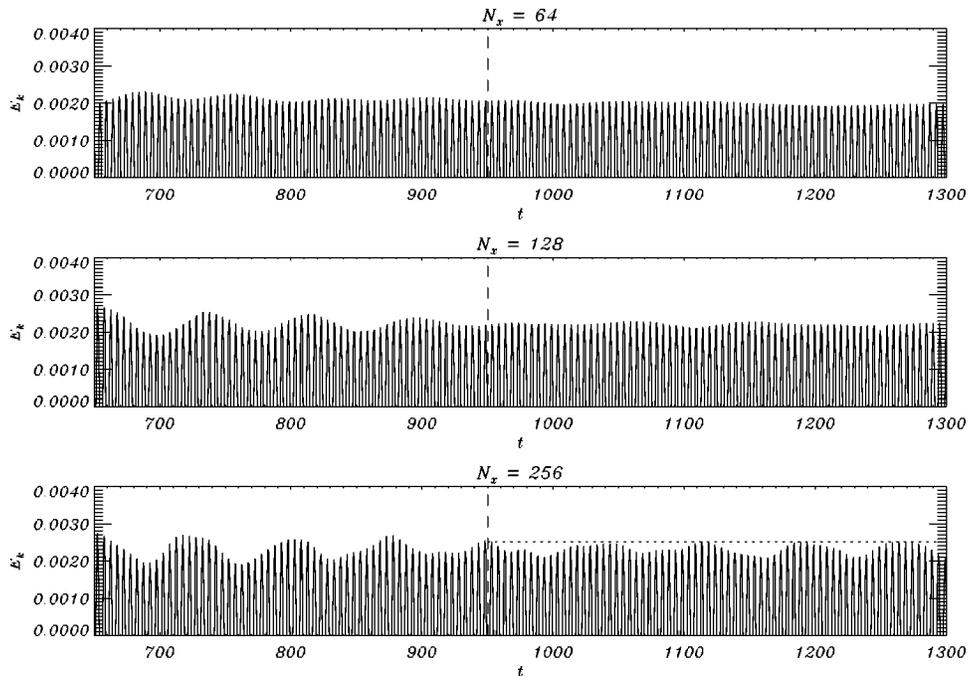

FIG. 2. Spatial Fourier component of the electric field E_k versus t for $k = 2\pi/L = 4$, $\epsilon = 0.1$, and for $N_x = 64$, $N_x = 128$, and $N_x = 256$, respectively.
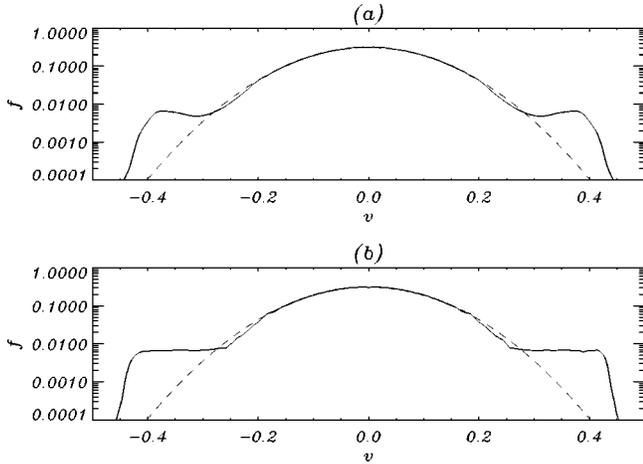
FIG. 3. Semilogarithmic plot of the EDF (averaged over x) versus v at $t=0$ (dashed line) and $t=1100$ (solid line) for $\epsilon=0.2$: (a) $L=2\pi/4$; (b) $L=2\pi$.

field amplitude starts to oscillate around a constant nonzero value is the same in all the simulations ($t_c \simeq 950$). The difference between the runs is that for bigger values of N_x, larger low-frequency oscillations in the electric field are observed. For $N_x=64$, the long-time amplitude is nearly constant. Moreover, the abscissas of the minima of the EDF (averaged over x) in the resonant region after a number of oscillations reach, in all the simulations with different N_x, the same constant value corresponding to the phase velocity of the wave, $\pm v_{ph}=\pm 0.31$, as seen in Fig. 3(a). The bumps in the EDF near these minima do not settle into a plateau.

In Fig. 4, the contour plot of the EDF in the resonant region is shown for $t=1200$, $\epsilon=0.1$, and for different values of the spatial resolution $N_x=64,128$, and 256. We note that the vortices become regular and the EDF and E_k become

time independent faster as the numerical dissipation in phase space increases (i.e., for smaller N_x). The filamentation in the vortices, corresponding to the low-frequency oscillations observed in the electric-field amplitude, disappears because of phase mixing on the grid scales $\Delta v=2v_{max}/N_v$ and $\Delta x=L/N_x$. Nevertheless, the overall structure that corresponds to a superposition of two traveling BGK waves is the same at large times in all the simulations, since t_c, v_{ph}, and the dimensions of the vortices do not change with the numerical resolution, as shown in Fig. 2, Fig. 3(a), and Fig. 4.

A similar conclusion has been obtained analytically in the small-amplitude limit in Ref. [3]. In fact, in this limit, the general solution for the asymptotic electric field E is a finite superposition of traveling waves plus higher order terms [see Eq. (9) of Ref. [3]]. Our numerical results show that the asymptotic electric field is given by a superposition of traveling ''averaged'' BGK waves, i.e., of stationary solutions in their own reference frame, also in the case of nonsmall amplitudes.

As long as the relative phase velocity Δv of the two BGK waves is sufficiently large, so that particles trapped in one wave feel only a high-frequency perturbation from the field of the other, we can consider the two BGK waves as independent [4]. This corresponds to the following condition on the field amplitude a_{fin}:

$$a_{fin} \ll k \ (\Delta v)^2, \tag{4.1}$$

which is well satisfied, in our case (see Table I) with $k(\Delta v)^2=k(2v_{ph})^2 \simeq 1.5$.

Eventually, the BGK waves will be affected by collisions. However, collisions will start to be important first on the smallest scales and will thus regularize the filamentary struc-
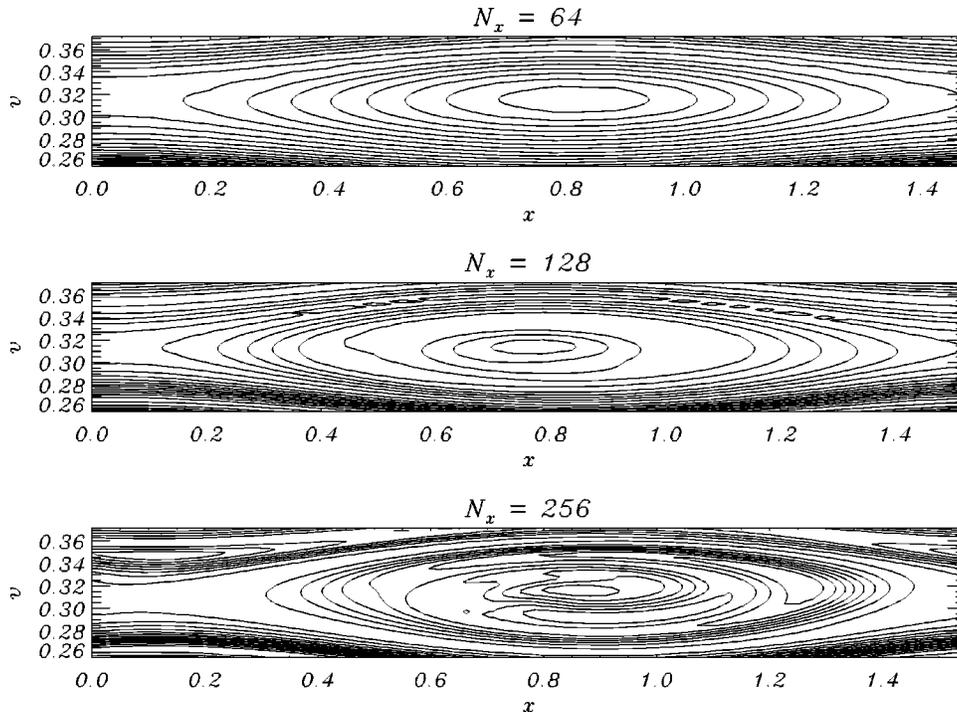

FIG. 4. Contour plot of the EDF in the resonant region at $t=1200$ for $\epsilon=0.1, L=\lambda$ and $N_x=64,128$, and 256, respectively.
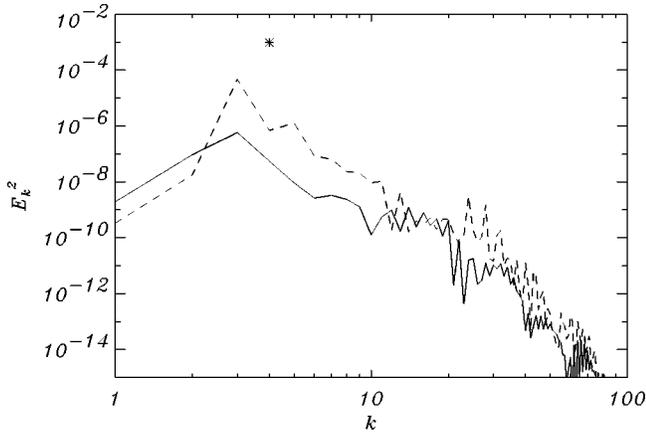
FIG. 5. Energy spectrum at $t=0$ (star), $t=375$ (dashed line), and $t=1100$ (solid line) for the simulation with $L=2\pi>\lambda$, $\epsilon=0.25$.

tures inside the vortices. The estimate of the ratio between the collision time at large scales t_l and at small scales t_s can be written as

$$t_l/t_s \simeq (v_{ph}N_v/2v_{max})^2, \qquad (4.2)$$

which for $v_{ph}=0.31$, $N_v=3000$, and $v_{max}=0.6$ gives $t_l/t_s \simeq 6 \times 10^5$.

More importantly, when longer-wavelength modes can be excited, the asymptotic electric field will be determined by the growth of upper and lower sideband waves [13]. In the simulations described so far, the length of the simulation box is set equal to the wavelength of the initial perturbation $L=\lambda=2\pi/k$. In order to study the long-time evolution of a more generic system, we have enlarged the simulation box, $L=2\pi>\lambda$, so as to allow for the presence of wave numbers smaller than the initially excited $k=4$ mode.

In Fig. 5, the energy spectrum is plotted for $\epsilon=0.25$ at different times. Initially, only the $k=4$ component is present and evolves as in the previous case, reaching a nearly constant amplitude. In the meantime, the two sideband modes $k=3$ and $k=5$ start to grow with equal rate. At $t_s \simeq 375$, the lower mode reaches the same level of the $k=4$ mode (dashed line in Fig. 5), which falls off abruptly. This evolution corresponds to four vortices, at the resonant velocity $v_{ph}=0.31$ in the interval L, which at $t_s \simeq 375$ become unstable and start to mix, as seen in Fig. 6. When the lower $k=3$ mode reaches the same level of the $k=4$ mode and becomes dominant, the $k=4$ mode decreases significantly so that three vortices are present in phase space and its overall resonant structure remains relatively ''coherent.''

At larger times, $t \simeq 1100$ (solid line in Fig. 5), other sideband Fourier components become important and many vortices are present at the same time in the resonant region, leading to an EDF that settles into a flat plateau, as can be seen in Fig. 3(b). The difference between the resonant velocities Δv of these vortices depends on the length of the simulation box. As this length increases, Δv becomes smaller and the condition (4.1) ceases to be valid, resulting in the overlapping of the vortices in phase space and in the chaotic motion of the particles in the resonant region.

The growth rate of the sideband instability increases with the wave amplitude, as can be seen in Fig. 7, with a power-law scaling between square root and linear, in agreement with Ref. [14]. Thus the lifetime of the BGK solution decreases with the wave amplitude and depends logarithmically on the initial noise in the $k \pm 1$ sideband Fourier components. We note that at ''large'' initial field amplitudes (in our case, for $a_{in}>0.025$, as shown in Fig. 7), the growth rate saturates.

Finally, we include the ion dynamics in the numerical code by integrating the corresponding Vlason-Poisson equations in order to verify whether the ion response can modify
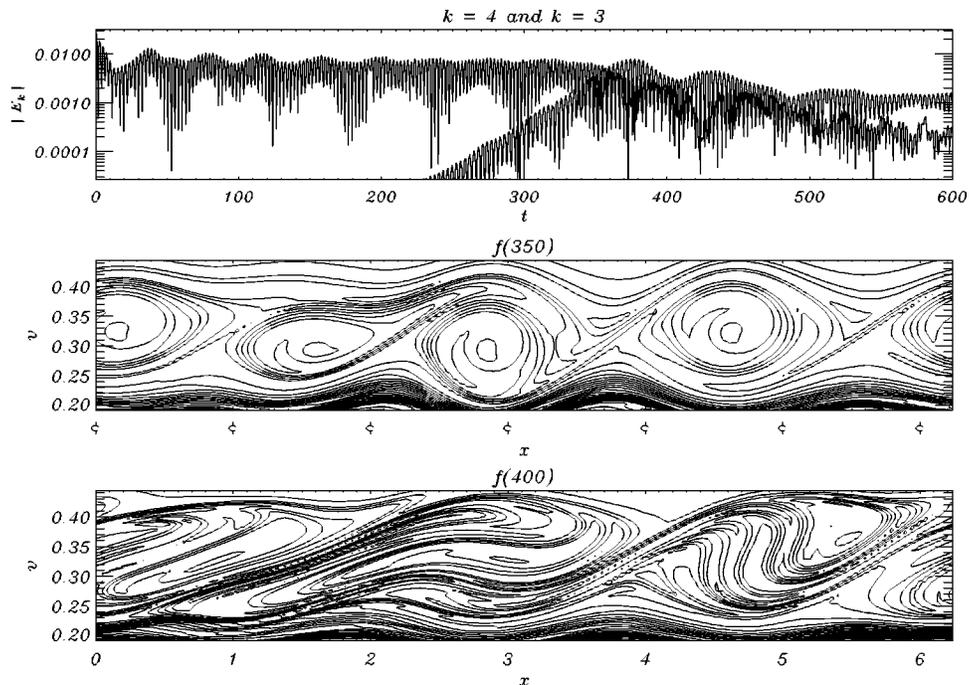

FIG. 6. Onset of the sideband instability ($\epsilon=0.25$): (top) Semilogarithmic plot of $|E_k|$ versus t for $k=4$ and $k=3$; (middle) contour plot of the EDF in the resonant region at $t=350$; and (bottom) at $t=400$.
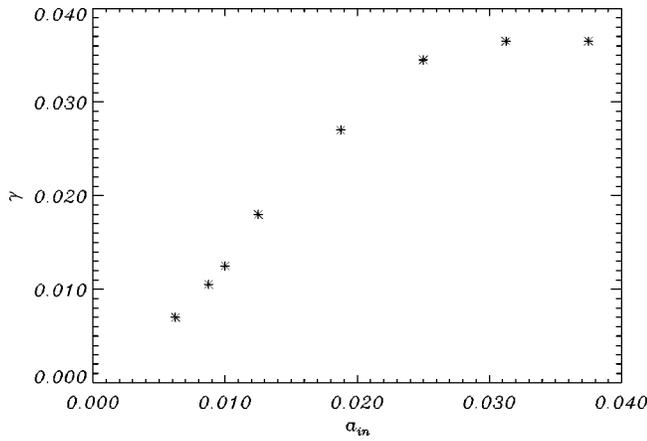
FIG. 7. Growth rate γ of the sideband modes versus the initial wave amplitude a_{in}.

the asymptotic evolution of the system described previously. In fact, the charge separation induced, for example, by ponderomotive effects (see Ref. [15] and references therein) is supposed to play a significant role in the asymptotic evolution of electrostatic waves. Typically, we investigate the plasma evolution up to $2500\omega_{pe}^{-1}$, which corresponds to $\simeq 58$ ion dynamics times. We find that the system dynamics is not affected by the ion motion, even for the (unrealistic) value of the mass ratio $m_i/m_e = 100$. In fact, the damping time t_d, the real part of the frequency ω, and the time t_s at which the sideband mode reaches the one that is initially excited do not change with respect to the case of fixed ions (i.e., they are $t_d = 7.7$, $\omega = 1.22$, and $t_s = 375$ for $\epsilon = 0.25$ and $k=4$, to be compared to the corresponding results in Table I and Fig. 6). After the initial damping of the wave, the field amplitude becomes small (of the order of a_{fin} listed in Table I) on a time scale t_p shorter than the ion dynamics time. By considering waves that do not resonate with the electrons and thus have a constant amplitude, we have verified that, for an initial field amplitude $a \simeq a_{fin}$, the ions do not play a significant role on the evolution of the system.

V. SUMMARY AND CONCLUSIONS

We have studied the long-time evolution of longitudinal perturbations in a spatially uniform collisionless plasma.

When the wavelength of the initially excited mode is equal to the simulation length $\lambda = L$, we have found that, in the limit of small wave amplitudes, our numerical results are in agreement with the analytical analysis performed in Ref. [3]. In particular, we have found that in this limit our numerical results agree with the analytical evaluated asymptotic electric-field amplitude a_{fin}, when the critical perturbation amplitude ϵ^*, which marks the transition between Landau's and O'Neil's scenario, is set to $\epsilon^* = 0.012$ in our parameter range (i.e., $k=4$ and Maxwellian equilibrium with $v_{th} = 0.1$). Moreover, for initial perturbation amplitudes such that $\epsilon > \epsilon^*$, we have found that the asymptotic solution is a superposition of two counterpropagating averaged BGK waves, also in the case of nonsmall amplitudes.

For $L > \lambda$, the onset of the sideband instability modifies the plasma evolution. The BGK waves become unstable when the amplitude of the daughter sideband mode reaches the amplitude of the initially excited mode. Thus, in this case, the BGK waves correspond to an intermediate regime, their lifetime decreasing with the wave amplitude.

Finally, we have verified that including the ion dynamics does not affect the asymptotic evolution of the system.

ACKNOWLEDGMENTS

[1] L. D. Landau, J. Phys. (Moscow) **10**, 25 (1946).

[2] T. O'Neil, Phys. Fluids **8**, 2255 (1965).

[3] C. Lancellotti and J.J. Dorning, Phys. Rev. Lett. **81**, 5137 (1998).

[4] M. Buchanan and J.J. Dorning, Phys. Rev. Lett. **70**, 3732 (1993); Phys. Rev. E **50**, 1465 (1994); **52**, 3015 (1995).

[5] M. Bernstein, J.M. Greene, and M.D. Kruskal, Phys. Rev. **108**, 546 (1957).

[6] M.B. Isichenko, Phys. Rev. Lett. **78**, 2369 (1997); C. Lancellotti and J.J. Dorning, *ibid.* **80**, 5236 (1998); M.B. Isichenko, *ibid.* **80**, 5237 (1998).

[7] G. Manfredi, Phys. Rev. Lett. **79**, 2815 (1997).

[8] M.V. Medvedev, P.H. Diamond, M.N. Rosenbluth, and V.I. Shevchenko, Phys. Rev. Lett. **81**, 5824 (1998).

[9] C.Z. Cheng and G. Knorr, J. Comput. Phys. **22**, 330 (1976).

[10] S.P. Gary, Phys. Fluids **10**, 570 (1967).

[11] R. Sugihara, K. Yamanaka, Y. Ohsawa, and T. Kamimura, Phys. Fluids **24**, 434 (1981).

[12] R. Sugihara and T. Kamimura, J. Phys. Soc. Jpn. **33**, 206 (1972); J. Canosa, Phys. Fluids **17**, 2030 (1974); J.J. Rasmussen, Phys. Scr. **T2/1**, 29 (1982).

[13] W.L. Kruer, J.M. Dawson, and R.N. Sudan, Phys. Rev. Lett. **23**, 838 (1969); M.V. Goldman, Phys. Fluids **13**, 1281 (1970); M.V. Goldman and H.L. Berk, *ibid.* **14**, 801 (1971).

[14] W.L. Kruer and J.M. Dawson, Phys. Fluids **13**, 2747 (1970).

[15] M. Lontano and F. Califano, Phys. Rev. E **61**, 4336 (2000).